ResearchGate

See discussions, stats, and author profiles for this publication at:
https://www.researchgate.net/publication/229171867

Direct dynamics simulation of the methanethiol cation decomposition

ARTICLE *in* CHEMICAL PHYSICS LETTERS · JUNE 2000

Impact Factor: 1.9 · DOI: 10.1016/S0009-2614(00)00591-1

CITATIONS
10

READS
19

4 AUTHORS, INCLUDING:

Emilio Martinez-Nuñez
University of Santiago de Compostela
85 PUBLICATIONS **1,018** CITATIONS
SEE PROFILE

Saulo A Vázquez
University of Santiago de Compostela
89 PUBLICATIONS **1,043** CITATIONS
SEE PROFILE

Available from: Emilio Martinez-Nuñez
Retrieved on: 21 January 2016

30 June 2000

ELSEVIER

Chemical Physics Letters 324 (2000) 88–94

CHEMICAL PHYSICS LETTERS

www.elsevier.nl/locate/cplett

Direct dynamics simulation of the methanethiol cation decomposition

E. Martínez-Núñez, A. Peña-Gallego, R. Rodríguez-Fernández, S.A. Vázquez *

Departamento de Química Física, Universidad de Santiago de Compostela, Santiago de Compostela E-15706, Spain

Received 1 April 2000; in final form 8 May 2000

Abstract

The dynamics of the unimolecular decomposition of the methanethiol radical cation (CH_3SH^+) was investigated by direct classical trajectories in which the interatomic forces were evaluated by semi-empirical AM1 calculations. At 170 kcal/mol, the methanethiol cation decomposition is found to be non-statistical. The abundances of product ions calculated for different initial conditions are in reasonable agreement with those determined experimentally. Our results corroborate that the coupling between the low- and high-frequency vibrational modes is weak in the methanethiol cation. © 2000 Elsevier Science B.V. All rights reserved.

1. Introduction

The success of the RRKM theory relies on the general fulfillment of its fundamental assumption that intramolecular energy redistribution is rapid as compared with the rate of reaction. However, deviations from RRKM behavior may occur when the initial excitation of the molecule involves a group of vibrational modes only. In such cases, if the vibrational modes are not strongly coupled, several decay regimes may appear. Such deviations correspond to what Bunker and Hase called apparent non-RRKM behavior [1].

In recent years, we have focussed on the study of unimolecular processes evolving in a non-RRKM fashion [2–9]. Among these studies, the decomposition of the methanethiol radical cation (CH_3SH^+) [8,9] is of particular interest on account of the amount of experimental data available [10–14]. Fenn et al. [10] have recently undertaken collisional activation studies of the fragmentation reactions of CH_3SH^+. They found that the decomposition dynamics is non-statistical and suggested that the lowest- and highest-frequency modes in the methanethiol cation are poorly coupled. Conversely, Kutina et al. [11] found agreement between their breakdown diagram and that obtained by RRKM calculations. However, as stated elsewhere [8], their RRKM calculations were based on assumed parameters and therefore their conclusions may be questionable. In addition, RRKM calculations bypass the dynamical details, which can be addressed with classical trajectory calculations. In fact, in a previous classical trajectory study [9], we obtained non-RRKM dynamics at energies ranging from 100 to 170 kcal/mol. The agreement between our classical dynamics and the experi-

* Corresponding author. Fax: +34-9-81-59-50-12; e-mail: qfsaulo@usc.es

0009-2614/00/$ - see front matter © 2000 Elsevier Science B.V. All rights reserved.
PII: S0009-2614(00)00591-1

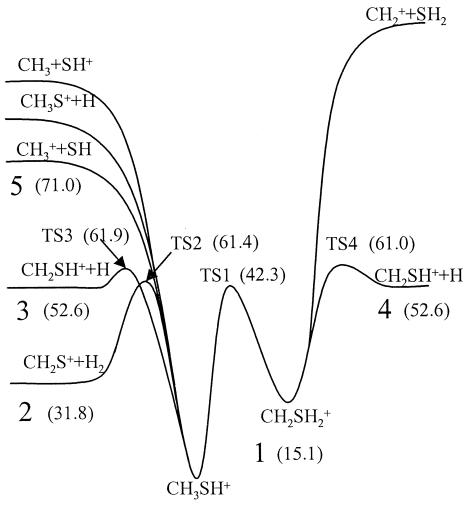

Fig. 1. Potential energy profile for rearrangement and decomposition reactions for CH_3SH^+. The reactions studied in this work are assigned by numbers and the corresponding energetics calculated by the AM1-SRP model are given in kcal/mol.

mental branching ratios was satisfactory and our calculations corroborated that the weak coupling between the low- and high-frequency vibrational modes together with a non-random initial energy preparation lead to non-statistical dynamics in the collisional activation experiment of Fenn et al. [10].

Our previous trajectory study was based on a reduced dimension analytical potential energy surface (PES) derived from experimental and theoretical data, and involved three decomposition channels only: the elementary reactions indicated by numbers 3 and 5 in Fig. 1, and that leading to $CH_3S^+ + H$. In the present Letter, we have explored the five lowest-energy elementary reactions by using a direct dynamics procedure [15–18] in which trajectories are integrated 'on the fly', without an analytical potential, by evaluating the energy and gradient directly from electronic structure theory. The trajectories are calculated by interfacing the classical trajectory program GENDYN [19] with the semi-empirical package MOPAC 7.0 [20,21] in which some of the original AM1 parameters [22] are substituted for specific reaction parameters (SRP) [16–18,23]. The characteristics of the lifetime distributions at a total energy of 170 kcal/mol will be discussed and the relative abundances of the product ions will be compared with those determined experimentally [10–12].

2. AM1-SRP semi-empirical model

We employed the AM1 Hamiltonian [22] in the MOPAC 7.0 [20,21] semi-empirical package, with some of the original parameters replaced for specific reaction parameters [16–18,23]. The use of specific reaction parameters was proposed by Truhlar and coworkers [23], who adjusted the parameters of a NDDO wave function to reproduce experimental or ab initio data for specific reactions. In this approach, fitting an analytical potential energy surface for a given system is replaced by finding specific electronic structure parameters for that reaction. The resulting model is referred to as AM1-SRP. The parameters modified to obtain appropriate energies, geometries, and frequencies for all the species involved in our calculations concerned one-electron integrals (U_{ss} and U_{pp}), two-electron one-center integrals (G_{ss}, G_{sp}, G_{pp}, G_{p2}, and H_{sp}), core-core repulsion range parameters (α), Slater orbital exponents (z_s and z_p), and resonance integral multipliers (β_s and β_p); they are listed in Table 1. Also listed for comparison are the original AM1 parameters. Our

Table 1
AM1 and AM1-SRP parameters [a]

Atom	Parameter	AM1 value	AM1-SRP value
H	U_{ss}	−11.396	−11.326
	β_s	−6.174	−5.654
	z_s	1.188	1.238
	α	2.882	3.032
	G_{ss}	12.848	12.888
C	U_{pp}	−39.614	−39.364
	β_s	−15.716	−16.556
	β_p	−7.719	−7.909
	α	2.648	2.608
	G_{ss}	12.230	12.100
	G_{sp}	11.470	11.650
	G_{p2}	9.840	9.820
S	U_{ss}	−56.694	−57.504
	U_{pp}	−48.717	−48.657
	β_p	−7.905	−7.845
	z_s	2.367	2.387
	G_{ss}	11.786	11.826
	G_{sp}	8.663	8.683

[a] Only those parameters that were changed in the AM1-SRP model PES are listed in the table.

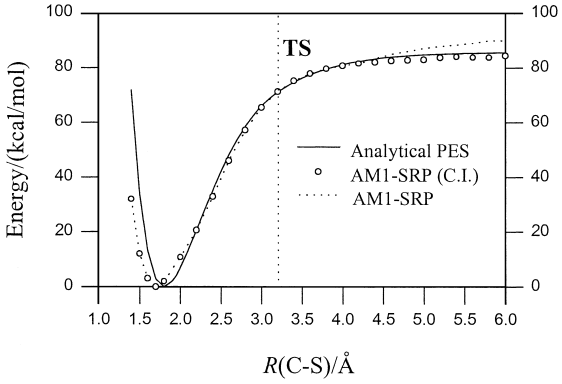

Fig. 2. C–S dissociation curves calculated by: our previous model PES [9] (solid line), the AM1-SRP model (dotted line), and the AM1-SRP model with a configuration interaction including the HOMO and the LUMO.

own ab initio data [8] was used in the reparameterization procedure [1].

It is well-known that the simplest molecular orbital methods do not reproduce a dissociation curve adequately. More elaborate treatments, such as configuration interaction (CI), are needed to appropriately describe bond dissociations. For the C–S dissociation channel, we have plotted in Fig. 2 the dissociation curves (up to 6 Å) obtained by our previous analytical PES [9], and those computed with the AM1-SRP model with and without invoking a CI calculation with the HOMO and the LUMO. As can be seen, there is a general agreement for the three curves (especially for the attractive region). Furthermore, and fortunately, both AM1-SRP curves coincide up to 4.5 Å, a distance longer than the location of the variational transition state (3.2 Å) calculated in our previous study [9]. On the other hand, the energetics for the remaining channels calculated with and without CI are very similar. Thus, for computational efficiency, we selected the simplest AM1-SRP model.

The criterion for obtaining a converged self-consistent field is that the energy of two successive SCF iterations differs by less than 10^{-6} kcal/mol. With such a criterion very good energy conservation is obtained during the trajectories. Forces on the nuclei are calculated analytically using the default Dewar–Liotard [24] package in MOPAC [2].

Fig. 3 shows the geometries of the stationary points located with the AM1-SRP model and Table 2 compares the relative energies of these stationary points with those obtained with our reported analytical PES [9] and with QCISD(T)/6-311G** calculations [8]. As shown in Table 2, there is a reasonable agreement between the ab initio and the AM1-SRP energy results. The major deviations are found for saddle point TS3 and the $CH_2SH_2^+$ minimum.

3. Trajectory computational details

The trajectories were initialized in two ways. First, the efficient microcanonical sampling (EMS) [25] with $J = 0$ was used to prepare a microcanonical ensemble at a total energy of 170 kcal/mol. The details of this sampling scheme are reported in our previous classical trajectory study [9].

In the second excitation scheme, a group of normal modes were selectively excited to obtain a total energy of 170 kcal/mol. Two ensembles were constructed in this way. In the first (referred to as L–F) the three lowest-frequency modes, corresponding to the torsion, CS stretch, and CSH bend, were initially excited. The second (called H–F) corresponds to an initial excitation of the three CH_3 stretching normal modes. Additionally, for each of the above three ensembles (EMS, L–F, and H–F), rotational energy was added around one of the three principal axes of inertia. Thus, for each kind of initial conditions two more ensembles were designed: one with 160 kcal/mol of vibrational energy plus 10 kcal/mol of *a*-axis rotational energy (these ensembles were called EMSa L–Fa, and H–Fa), and the other with the same vibrational energy and 5 kcal/mol in each of the other two rotational axes (named by EMSbc, L–Fbc, and H–Fbc).

The trajectories were integrated by using a fourth-order Runge–Kutta–Gill routine. At each step

[1] The AM1-SRP parameters were selected to model the ab initio relative energies (mainly), geometries, and frequencies given in Ref. [8] for the relevant species involved in this study.

[2] To obtain more accurate first derivatives, the parameter THROLD in subroutine DERNVO was set to 10^{-4}. Lower values do not significantly affect the derivatives.

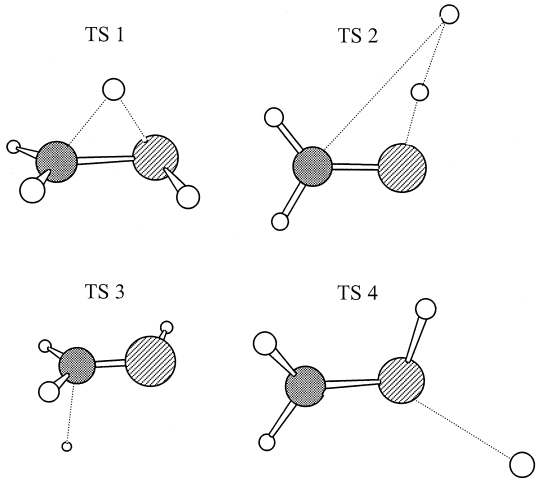

Fig. 3. Transition states located in this work on the AM1-SRP surface.

of the integration the Schrödinger equation is solved for electronic energies and forces on the nuclei. Once a converged SCF has been obtained, the first derivatives of the energy with respect to the Cartesian coordinates are evaluated analytically within MOPAC 7.0. The trajectories were integrated with a fixed step size of 0.1 fs, which ensures an energy conservation of at least four significant figures. The trajectories were propagated until one of the reactions occurred or 4 ps elapsed. Following our previous criterion [9], the lifetime of an individual trajectory was taken to be the integration time for the first passage through the top of the barrier. The criterion for terminating a trajectory resulting in C–S dissociation was that the C–S bond was at least 3.2 Å (this is the distance for the variational transition state obtained in our previous statistical calculations [9]).

Each ensemble comprises 500 trajectories, and the integration of a typical 300 fs trajectory required ≈ 4630 cpu seconds on a SUN HPC4500 computer. Additionally, for the Markov walk involved in the EMS initialization, 5×10^5 SCF calculations were required before the first trajectory and 10^4 between each trajectory.

Finally, the microcanonical rate constants were obtained from the lifetime distribution, which is the probability that decomposition occurs in the time interval t to $t + \mathrm{d}t$,

$$P(t) = 1/N(0)\left[N(t)\right]$$

where $N(t)$ is the concentration at time t. The $t = 0$ intercept of $P(t)$ gives the RRKM rate constant for the EMS ensemble. The RRKM rate constants thus obtained will be compared with those calculated in our previous classical trajectory study [9], and the relative abundance of product ions with those obtained experimentally [10–12].

4. Results

For all the ensembles studied, a double exponential was required to fit the lifetime distributions

Table 2
Stationary points on the CH_3SH^+ surface located with a model potential, and ab initio and AM1-SRP wave functions.

Stationary point	Ab initio [a]		Analytical PES [c]		AM1-SRP [d]	
	Sym	E_{rel} [b]	Sym	E_{rel}	Sym	E_{rel} [b]
CH_3SH^+	C_s	0.0	C_s	0.0	C_s	0.0
$CH_2SH_2^+$	C_s	21.5			C_s	15.1
$CH_2SH^+ + H$	C_s	54.0	C_s	54.4	C_s	52.6
$CH_2S^+ + H_2$	C_s	34.4			C_s	31.8
TS1	C_1	45.2			C_1	42.3
TS2	C_s	56.2			C_s	61.4
TS3	C_1	55.2	C_1	56.0	C_1	61.9
TS4	C_1	57.0			C_1	61.0

[a] QCISD(T) energies from Ref. [8].
[b] Relative energies in kcal/mol, excluding zero-point energy.
[c] Model PES from Ref. [9].
[d] This work.

$P(t)$. For the sake of example, we depicted in Fig. 4 the lifetime distributions for ensembles EMS, L–F, and H–F. The double exponential decay for the EMS ensemble suggests that phase space bottlenecks govern the rate of intramolecular vibrational energy redistribution. As a consequence, the microcanonical ensemble is not maintained during the decomposition (intrinsic non-RRKM behavior) [1]. Similar behavior was found in our previous trajectory study at the same energy. The characteristics of the lifetime distributions are collected in Table 3. Also listed for comparison are the results obtained in Ref. [9]. For the microcanonical ensemble (EMS), the rate constant is calculated to be 4.0 ps^{-1}, a value similar to those calculated previously by classical trajectories and statistical calculations with an analytical PES (4.6 ps^{-1} for both types of calculation) [9]. Also seen from Table 3 is the fact that the rate constants depend very much on the way in which the molecule is initially excited, that is, apparent non-RRKM is clearly exhibited [1].

Table 4 lists the relative abundances of product ions obtained in this work at 170 kcal/mol, in our previous trajectory study [9], and in several experimental investigations (values for the energy range 165–168 kcal/mol including the zero-point energy) [10–12]. The experimental abundances shown in the table for CH_2SH^+ include the percentage of HCS^+ ions, which are expected to be a product of a further dissociation of internally excited CH_2SH^+ [10]. Also shown in Table 4 is the percentage of reactive trajectories undergoing isomerization. The abundances calculated under random vibrational excitation (EMS) are in reasonable agreement with those determined by charge-exchange [12] and photoionization mass spectrometry [11], experimental techniques with which the methanethiol cation is ex-

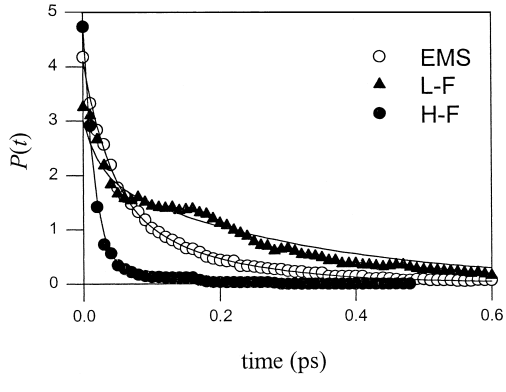

Fig. 4. Lifetime distributions for ensembles EMS (open circles), L–F (triangles), and H–F (circles). The double exponential fit is also shown.

Table 3
Characteristics of the lifetime distributions obtained at 170 kcal/mol.

	Rate constants (ps^{-1})	k_{RRKM} (ps^{-1})
EMS	13 (29%); 0.1 (71%)	4.0
EMSa	10 (34%); 0.1 (66%)	
EMSbc	9 (37%); 0.1 (63%)	
L-F	5 (53%); 0.04 (47%)	
L–Fa	4 (61%); 0.02 (39%)	
L–Fbc	7 (46%); 0.1 (54%)	
H–F	57 (8%); 0.04 (92%)	
H–Fa	51 (9%); 0.2 (91%)	
H–Fbc	47 (10%); 0.2 (90%)	
Analyt. PES [a]	13 (25%); 2 (75%)	4.6
Analyt. PES [b]		4.6

[a] Trajectory calculations with an analytical PES from Ref. [9].
[b] Statistical calculations with an analytical PES from Ref. [9].

Table 4
Relative abundance of the relevant product ions [a]

	CH_2SH^+	CH_2S^+	CH_3^+	Isomer [f]
EMS	90	2	8	57
EMSa	90	4	6	64
EMSbc	80	4	16	59
L–F	26	4	70	39
L–Fa	32	4	64	46
L–Fbc	22	3	75	38
H–F	99	1	0	9
H–Fa	100	0	0	13
H–Fbc	98	1	1	14
Anal. PES [b]	88	– [e]	10	–
Experiment [c]	22	1	76	
Experiment [d]	90 (87)	6 (8)	3 (3)	

[a] Theoretical values calculated at 170 kcal/mol. Experimental data obtained in the energy range 165–188 kcal/mol (zero-point energy included). Experimental abundances for CH_2SH^+ include the percentage of HCS^+ ions (see text).
[b] Results employing the analytical PES of Ref. [9] under EMS initialization.
[c] Results from Ref. [10].
[d] Results from Refs. [11,12](values in parentheses).
[e] The reaction channel leading to this ion was not considered in this model.
[f] Percentage of reactive trajectories undergoing isomerization.

pected to be prepared with a statistical distribution of the internal energy. The dominant product ion is CH_2SH^+ (90%). Since the classical trajectories predict intrinsic non-RRKM behavior at 170 kcal/mol, our results suggest that the decomposition of the methanethiol cation in the above experiments might evolve non-statistically or close to the statistical limit.

Under selective excitation of the stretching normal modes associated with the methyl group (high-frequency modes), the decomposition leads practically to CH_2SH^+ only. In addition, the percentage of reactive trajectories undergoing isomerization is substantially reduced, as expected.

When the energy is selectively deposited in the low-frequency modes (torsion, CS stretch, and CSH bend), the relative abundance of CH_2SH^+ decreases dramatically and, conversely, the formation of $CH_3^+ + SH$ (i.e., channel 5) becomes dominant. This result agrees with the experimental observations made by Fenn et al. [10] and corroborates their conclusion that collisional activation prepares the methanethiol cation with a non-random distribution of the internal energy (the energy is preferentially deposited in the low-frequency C–S stretch), leading to non-statistical behavior (more specifically, apparent non-RRKM behavior). On the other hand, the percentage of reactive trajectories undergoing isomerization (39% for ensemble L–F) decreases with respect to the EMS value (57%) because channel 3 is now more effective.

Finally, our results predict that rotational motion may influence the abundances of the product ions. Specifically, the percentage of the CH_3^+ ion decreases under *a*-axis rotation whereas it increases under rotation around the other axes of inertia. For example, the values for ensembles L–F, L–Fa, and L–Fbc are calculated to be 70%, 64%, and 75%, respectively. In addition, for the low-frequency ensembles, the percentage of CH_2SH^+ increases significantly under *a*-axis rotation (32% for L–Fa versus 26% for L–F) and decreases under *b*-axis and *c*-axis rotation (22%). These trends may be explained by simple classical mechanics considerations. Since the *a*-axis is almost coincident with the C–S bond, rotation around the other axes causes a centrifugal force along this bond, which increases the yield of CH_3^+ ions. On the contrary, *a*-axis rotation promotes C – H scissions because of an important component of the centrifugal force along this bond. Also, *a*-axis rather than *b*- or *c*-axis rotation is expected to promote isomerizations (see Table 4). To sum up, the calculations show that the abundances of the product ions can vary significantly depending on how the methanethiol cation is initially prepared.

Acknowledgements

We thank 'Centro de Supercomputación de Galicia' CESGA for helping us with the interfacing between MOPAC and GENDYN and for time allocation for the calculations. We are pleased to acknowledge financial support of this research from Xunta de Galicia (XUGA20903A98). A.P.-G. also thanks Xunta de Galicia for a grant.

References

[1] D.L. Bunker, W.L. Hase, J. Chem. Phys. 59 (1973) 4621.
[2] E. Martínez-Núñez, S.A. Vázquez, J. Chem. Phys. 107 (1997) 5393.
[3] E. Martínez-Núñez, S.A. Vázquez, J. Chem. Phys. 109 (1998) 8907.
[4] E. Martínez-Núñez, S.A. Vázquez, J. Chem. Phys. 111 (1999) 10501.
[5] E. Martínez-Núñez, S.A. Vázquez, Chem. Phys. Lett. 310 (1999) 209.
[6] A. Peña-Gallego, E. Martínez-Núñez, S.A. Vázquez, J. Chem. Phys. 110 (1999) 11323.
[7] E. Martínez-Núñez, S.A. Vázquez, Chem. Phys. Lett. 316 (2000) 471.
[8] E. Martínez-Núñez, S.A. Vázquez TEOCHEM, in press.
[9] E. Martínez-Núñez, S.A. Vázquez, J. Phys. Chem. A 103 (1999) 9783.
[10] P.T. Fenn, Y.-J. Chen, S. Stimson, C.Y. Ng, J. Phys. Chem. A 101 (1997) 6513.
[11] R.E. Kutina, A.K. Edwards, J. Berkowitz, J. Chem. Phys. 77 (1974) 5508.
[12] B.-Ö. Jonsson, J. Lind, J. Chem. Soc. Faraday Trans. 2 (1974) 1399.
[13] S. Nourbaksh, K. Norwood, H.-M. Yin, C.-L. Liao, C.Y. Ng, J. Chem. Phys. 95 (1991) 945.
[14] Y.-S. Cheung, C.-W. Hsu, J.-C. Huang, W.-K. Li, S.-W. Chiu, Int. J. Mass. Spectrom. Ion Process. 13 (1996) 159.
[15] J.M. Millam, V. Bakken, W. Chen, W.L. Hase, H.B. Schlegel, J. Chem. Phys. 111 (1999) 3800.
[16] K. Bolton, W.L. Hase, G.H. Peslherbe, in: D.L. Thompson (Ed.), Modern Methods for Multidimensional Dynamics

Computation in Chemistry, World Scientific, Singapore, 1998, p. 143.
[17] C. Doubleday Jr., K. Bolton, W.H. Hase, J. Phys. Chem. A 102 (1998) 3648.
[18] C. Doubleday Jr., K. Bolton, G.H. Peslherbe, W.H. Hase, J. Am. Chem. Soc. 118 (1996) 9922.
[19] D.L. Thompson, GENDYN program.
[20] J.P.P. Stewart, MOPAC 7.0, a General Molecular Orbital Package. QCPE 1993, 455.
[21] J.P.P. Stewart, J. Comput. Chem. 10 (1989) 209.
[22] M.J.S. Dewar, E.G. Zoebish, E.F. Healy, J.P.P. Stewart, J. Am. Chem. Soc. 107 (1985) 3902.
[23] A. Gonzalez-Lafont, T. Truong, D.G. Truhlar, J. Phys. Chem. 95 (1991) 4618.
[24] M.J.S. Dewar, D.A. Liotard, J. Mol. Struct. (THEOCHEM) 206 (1990) 123.
[25] G. Nyman, S. Nordholm, H.W. Schranz, J. Chem. Phys. 93 (1990) 6767.